J. Fluid Mech. (1978), *vol.* 84, *part* 1, *pp.* 55–77
Printed in Great Britain

Effects of hydrogen impurities on shock structure and stability in ionizing monatomic gases. Part 1. Argon

By I. I. GLASS AND W. S. LIU
Institute for Aerospace Studies, University of Toronto, Ontario, Canada M3H 5T6

(Received 8 February 1977)

At shock Mach numbers $M_s \sim 16$ in pure argon with initial pressures $p_0 \sim 5$ torr and final electron number densities $n_e \sim 10^{17}\,\mathrm{cm}^{-3}$, the translational shock front in a 10×18 cm hypervelocity shock tube develops sinusoidal instabilities which affect the entire shock structure including the ionization relaxation region, the electron-cascade front and the final quasi-equilibrium state. By adding a small amount of hydrogen ($\sim 0{\cdot}5\,\%$ of the initial pressure), the entire flow is stabilized. However, the relaxation length for ionization is drastically reduced to about one-third of its pure-gas value. Using the familiar two-step collisional model coupled with radiation-energy loss and the appropriate chemical reactions, it was possible to deduce from dual-wavelength interferometric measurements a precise value for the argon–argon collisional excitation cross-section $S^*_{\mathrm{Ar\,Ar}} = 1{\cdot}0 \times 10^{-19}$ cm^2/eV with or without the presence of a hydrogen impurity. The reason for the success of hydrogen, and not other gases, in bringing about stabilized shock waves is not clear. It was also found that the electron-cascade front approached the translational-shock front near the shock-tube wall. This effect appears to be independent of the wall material and is not affected by the evolution of adsorbed water vapour from the walls or by water vapour added deliberately to the test gas. The sinusoidal instabilities investigated here may offer some important clues to the abatement of instabilities that lead to detonation and explosions.

1. Introduction

A fair number of papers exist that deal with measurements and theoretical calculations of ionization and relaxation phenomena in argon–plasma flows. Although many of these papers are concerned with the determination of the atom–atom collision excitational cross-section constant, its value has yet to be determined accurately. For example, it is not certain whether it is dependent on the shock Mach number, the initial pressure or on other factors. Harwell & Jahn (1964) employed a transverse microwave probe to determine the cross-section $S^*_{\mathrm{Ar\,Ar}} = 7 \times 10^{-19}\,\mathrm{cm}^2/\mathrm{eV}$ for argon atom–atom excitational collisions. Morgan & Morrison (1965) have made a theoretical reassessment of the ionization mechanism and referred to earlier experimental measurements. They showed that a best-fit curve to the ionization relaxation-time measurements of Petschek & Byron (1957) was obtained by reducing Harwell & Jahn's value by a factor of ten. Kelly (1966) reduced the impurity level for his experiments and obtained a value of $1{\cdot}2 \times 10^{-19}\,\mathrm{cm}^2/\mathrm{eV}$, which is in very good agreement with the present values of $1{\cdot}0 \times 10^{-19}\,\mathrm{cm}^2/\mathrm{eV}$ for $M_s \sim 16$ and $p_0 \sim 5$ torr and $2 \times 10^{-19}\,\mathrm{cm}^2/\mathrm{eV}$

for $M_s \sim 13$ and $p_0 \sim 3$ torr. McLaren & Hobson (1968) used double electrostatic probes to measure the ionization rate and took into account the flow non-uniformities resulting from the boundary-layer growth on the shock-tube wall. They obtained a value of $2{\cdot}5 \times 10^{-20}$ cm^2/eV. Enomoto (1973) has shown that the laminar wall boundary layer can significantly reduce the ionization relaxation length behind a shock wave in tubes of smaller cross-section. Merilo & Morgan (1970) obtained excellent agreement between theory and experiment by using Kelly's value for the argon atom–atom excitational cross-section constant and a lower value for the argon electron–atom excitational cross-section constant. Other experiments also were made with argon to evaluate the initial ionization process. However, the excitational cross-section constant for argon atom–atom collisions was not uniquely determined.

The effect of impurities in the test gas on the structure of shock waves was studied initially by Morgan & Morrison (1965) using a relatively simple theory. Harwell & Jahn (1964) found that the effect of impurities on the initial ionization rate decreased rapidly with temperature, and that for an impurity level less than 1 in 10^4 there was no significant effect. However, Petschek & Byron (1957) indicated a dependence of the ionization time on impurity levels as low as 1 part in 10^5 in the temperature range 10 000–30 000 °K. Schultz-Grunow (1975) studied shock-wave structure in diatomic binary mixtures experimentally by electron fluorescence and analytically by a gas-kinetic four-fluid model. He found that there is a strong influence of O_2 impurity on the ionization of N_2.

Bristow & Glass (1972) describe some experiments in argon containing 0·4 % molecular hydrogen (by partial pressure). They found that a hydrogen impurity could readily stabilize the translational shock front, the relaxation region and the quasi-uniform region behind the shock wave by removing the sinusoidal-type oscillations. In addition, they noted that a hydrogen impurity significantly reduced the shock-wave relaxation length. It has also been observed that the electron-cascade front rapidly approaches the translational front near the wall. Although the shrinkage in the relaxation length can be readily accounted for kinetically, the reasons why hydrogen can stabilize the shock transition and the close approach of both fronts near the wall are not understood as yet.

The present study deals basically with: (i) an accurate interferometric determination of the excitational cross-section constant for argon atom–atom collisions in the relaxation zone over ranges of the initial shock Mach number and pressure of $13 < M_s < 18$ and $3{\cdot}1 < p_0 < 5{\cdot}2$ torr; (ii) an investigation of the effects of radiation on the relaxation zone and the quasi-equilibrium zone; (iii) an experimental and analytical determination of the effects of adding a small hydrogen impurity to the argon test gas on the relaxation zone and shock-wave stability; (iv) a qualitative understanding of the behaviour of the electron-cascade front near the wall.

2. Theoretical considerations

The conservation equations for a one-component plasma were formulated and discussed by Appleton & Bray (1964). Sherman (1960) investigated shock structure in a two-component mixture on the basis of continuum theory using the assumption of equal temperatures for the components. In this study, in order to simplify the calculations, it is assumed that the heavy particles of the two-component mixture of ionized

gases have the same temperatures and velocities. As the impurity level is small the errors arising from neglecting the kinetic energy and momentum transfer between two types of heavy particles should be small. Jaffrin (1965) showed that the kinetic energy transfer and momentum transfer between the heavy particles of one kind of plasma for frozen ionization are indeed very small. The governing equations for a two-component mixture of plasmas may be written as

$$(n_{a1}+n_{e1})\,u = n_{01}\,u_{01}, \tag{1}$$

$$(n_{a2}+n_{e2})\,u = n_{02}\,u_{02}, \tag{2}$$

$$\sum_{j=1}^{2}\{m_{aj}(n_{aj}+n_{ej})\,u^2+n_{ej}\,kT_e+(n_{aj}+n_{ej})\,kT_a\} = \sum_{j=1}^{2}\{m_{aj}\,n_{0j}\,u_{0j}^2+n_{0j}\,kT_{0j}\}, \tag{3}$$

$$\sum_{j=1}^{2}\left\{\frac{d}{dx}\left[\tfrac{1}{2}m_{aj}(n_{aj}+n_{ej})\,u^3+\tfrac{5}{2}(n_{aj}+n_{ej})\,kT_a\,u+\tfrac{5}{2}n_{ej}\,kT_e\,u+n_{ej}\,k\theta_j\,u\right]\right\} = -\sum_{j=1}^{2}(Q_{Rj}), \tag{4}$$

$$\tfrac{3}{2}n_e\,uk\frac{dT_e}{dx}+n_e\,kT_e\frac{du}{dx} = \sum_{j=1}^{2}(\eta_j+\phi_j), \tag{5}$$

$$d(n_{e1}\,u)/dx = \dot{n}_{e1}, \quad d(n_{e2}\,u)/dx = \dot{n}_{e2}, \tag{6), (7}$$

where n is the number density, u the velocity, T the temperature, k the Boltzmann constant, m the mass, θ the ionization temperature, Q_R the rate of radiant-energy loss, η the rate at which thermal energy is given to the free electrons by elastic collisions, ϕ the rate at which thermal energy is given to the free electrons by inelastic collisions and bremsstrahlung, and $\dot{n}_e$ the production rate of electron number density. Subscripts a, e, j ($j = 1, 2$) and 0 denote atom, electron, type of plasma mixture and initial conditions before the shock front, respectively. The total electron number density n_e is the sum of the electron number densities produced by each kind of atom (i.e. $n_e = n_{e1}+n_{e2}$). In the above equation, the effects of thermal conductivity and electron diffusion have been neglected. Any numerical solution of (1)–(7) will depend on the model adopted to describe the atomic processes ($\dot{n}_e$, η and ϕ) and the radiant-energy loss (Q_R).

It was shown by Petschek & Byron (1957) that excitation to the first state is rate-controlling for the overall ionization process. We assume that atoms in the ground level are excited to the first excitation level by collisions with other particles, then the excited atoms are ionized by subsequent collisions. The rates of reactions among levels higher than the first are assumed to be infinite, i.e. every excitation level is assumed to be in thermal equilibrium with the electrons in the entire relaxation zone. This assumption was also made by Oettinger & Bershader (1967) in studying radiation cooling of an argon plasma. The two-step model of Hoffert & Lien (1967) describing the electron production rate $\dot{n}_e$ and the assumption of a linear dependence of excitation cross-section on the relative kinetic energy are adopted herein. Photo-ionization and radiative recombination play very minor roles in the production of initial electrons and are neglected in the calculations.

The electron–atom inelastic collision cross-section constant of $4{\cdot}9\times10^{-18}\,\mathrm{cm^2/eV}$ for argon obtained more recently by Zapesochnyi & Felston (1966) is used in the present calculations. Values obtained by Belozerov & Measures (1969) are used for the excitational cross-section constants for the hydrogen atom: $3{\cdot}57\times10^{-18}\,\mathrm{cm^2/eV}$ for atom–atom collisions and $5{\cdot}1\times10^{-17}\,\mathrm{cm^2/eV}$ for electron–atom collisions.

The rate of radiant-energy loss (Q_R) consists of the rates of energy loss by continuum radiation (Q_C) and by line radiation (Q_B). The continuum radiation in a plasma is caused by recombination processes (free-bound radiation) and free–free transitions. Under the assumption of local temperature equilibrium, Q_C is given by (Oettinger & Bershader 1967)

$$Q_C = \frac{64\pi^{\frac{3}{2}}e^6}{3\times 6^{\frac{1}{2}}m_e^{\frac{3}{2}}c^3hk^{\frac{1}{2}}}\frac{n_e^2}{T_e^{\frac{1}{2}}}(h\nu_c + kT_e)\bar{g}Z_{\text{eff}}^2, \tag{8}$$

where e is the electron charge, h the Planck constant, c the speed of light, ν_c the cut-off frequency, $\bar{g}$ the Gaunt factor and Z_{eff} the effective nuclear charge. Equation (8) is known as the Kramers–Unsold equation.

For an optically thin plasma, the energy loss due to bound–bound transition can be written as (Kamimoto, Teshima & Nishimura 1972)

$$Q_B = \sum_k n_a(k)\,A_{k,k-1}(E_k - E_{k-1})\exp\{-(E_k - E_{k-1})/kT_e\}, \tag{9}$$

where E_k is the energy level of the kth excited state of an atom, $n_a(k)$ the number density of atoms at the kth excited state and $A_{k,k-1}$ a radiative transition rate coefficient. From the assumption of a two-step model, $n_a(k)$ is given by

$$n_a(k) = \frac{g_k}{2g_I}\left(\frac{h^2}{2\pi m_e kT_e}\right)^{\frac{3}{2}} n_e^2 \exp\{(k\theta - E_k)/kT_e\}, \tag{10}$$

where g_k and g_I are the atomic statistical weights of the kth level and for ionization, respectively.

In the present calculation, for simplicity we use $\bar{g} = 1$. Oettinger & Bershader (1967) used $Z_{\text{eff}}^2 = 1{\cdot}5$ for argon. Recently, Meiners & Weiss (1976) have found that for argon $Z_{\text{eff}}^2 = 1{\cdot}67$ is the most probable value for the range $T_e = 10\,500$–$12\,500\,^\circ\text{K}$ and $n_e = 0{\cdot}4$–$1{\cdot}7\times 10^{17}\ \text{cm}^{-3}$. Their value was used here and agrees well with two values obtained by Schultz-Guide (1970). Hollenbach & Salpeter (1969) have proposed a ladder-climbing model for the atom–atom ionization rates. They have tabled the effective rates $A_{k,k-1}$ of radiative transition for an argon plasma. However, their values of $A_{k,k-1}$ are smaller than the values obtained by Horn (1966) by a factor of ten. Horn, Wong & Bershader (1967) have found that the portion of line-radiation loss in the total radiation energy loss was about half for the present conditions. Consequently, some of the $A_{k,k-1}$ values given by Hollenbach & Salpeter (1969) were multiplied by a factor of ten in the present calculations. Since the impurity level of hydrogen used in the experiments was small, the rate of radiant-energy loss by line radiation for the hydrogen plasma is assumed equal to that due to continuum radiation. This assumption is crude in general but should give rise to a very small error in the present calculations.

The elastic energy transfer rate η is the sum of the rates at which thermal energy is given to the free electrons by electron–atom elastic collisions and by electron–ion elastic collisions: $\eta = \eta_{ea} + \eta_{ei}$, where

$$\eta_{ea} = 6\times 2^{\frac{1}{2}} n_e n_a \left(\frac{m_e kT_e}{\pi}\right)^{\frac{1}{2}} \frac{Q_{ea}}{m_a} k(T_a - T_e), \tag{11}$$

$$\eta_{ei} = 6\times 2^{\frac{1}{2}} n_e^2 \left(\frac{m_e kT_e}{\pi}\right)^{\frac{1}{2}} \frac{Q_{ei}}{m_a} k(T_a - T_e), \tag{12}$$

where Q_{ea} and Q_{ei} are the momentum transfer cross-sections between electrons and atoms and between electrons and ions, respectively. The values of Q_{ea} for argon were calculated by Devoto (1967) using the momentum transfer cross-section determined by Frost & Phelps (1964). The approximate value of Q_{ea} for argon found by curve fitting is (Enomoto 1973)

$$Q_{ea} = \begin{cases} (0{\cdot}713 - 4{\cdot}5 \times 10^{-4} T_e + 1{\cdot}5 \times 10^{-7} T_e^2) \times 10^{-16}\ \text{cm}^2 \text{ for } T_e < 3000\ ^\circ K, \\ (-0{\cdot}488 + 3{\cdot}96 \times 10^{-4} T_e) \times 10^{-16}\ \text{cm}^2 \text{ for } T_e \geqslant 3000\ ^\circ\text{K}. \end{cases} \tag{13}$$

For the hydrogen atom, Q_{ea} is expressed (Belozerov & Measures 1969) as

$$Q_{ea} = \frac{7{\cdot}12 \times 10^{-15}}{\pi^{\frac{1}{2}}} \left(\frac{m_e^2}{m_{a\text{H}}}\right)\left(\frac{2kT_e}{m_e}\right)^{\frac{3}{2}} \left(\frac{T_a}{T_e} - 1\right) \times \left[1 - 3\frac{T_R}{T_e} + \exp\left(-\frac{T_R}{T_e}\right)\left(\frac{T_R}{2T_e} + 2 + 3\frac{T_e}{T_R}\right)\right], \tag{14}$$

where $T_R = E_R/k$, $E_R = 14$ eV and $m_{a\text{H}}$ is the mass of the hydrogen atom.

The momentum transfer cross-section Q_{ei} between electrons and ions is given by

$$Q_{ei} = \frac{2\pi e^4}{9(kT_e)^2} \ln\left(\frac{9k^3T_e^3}{4\pi e^6 n_e}\right). \tag{15}$$

The inelastic energy transfer rate ϕ is the sum of the rates at which thermal energy is given to the free electrons by electron–atom and electron–ion–electron inelastic collisions (ϕ_{ea}) and by bremsstrahlung (ϕ_R). For the two-step model, ϕ_{ea} is given by

$$\phi_{ea} = -(\dot{n}_e)_e (k\theta + \tfrac{3}{2}kT_e), \tag{16}$$

where $(\dot{n}_e)_e$ is the net rate of production of electron density by electron-catalyzed reactions. Oettinger & Bershader (1967) give ϕ_R as

$$\phi_R = \frac{8\pi}{6^{\frac{1}{2}}} \frac{n_e^2 e^6 kT_e}{m_e^2 c^3 h} \left(\frac{8\pi m_e}{kT_e}\right)^{\frac{1}{2}}. \tag{17}$$

Chang (1966) has shown that the relaxation length for dissociation of hydrogen molecules is very small compared with that of ionization, therefore it is assumed that the ionization of the hydrogen molecules behind a strong shock starts effectively after the dissociation is complete. The following reactions are considered for the collisional ionization processes:

$$\text{Ar} + \text{Ar} \rightleftharpoons \text{Ar}^+ + \text{Ar} + \text{e}, \tag{18a}$$

$$\text{Ar} + \text{e} \rightleftharpoons \text{Ar}^+ + \text{e} + \text{e}, \tag{18b}$$

$$\text{Ar} + \text{H} \rightleftharpoons \text{Ar}^+ + \text{H} + \text{e}, \tag{18c}$$

$$\text{H} + \text{Ar} \rightleftharpoons \text{H}^+ + \text{Ar} + \text{e}, \tag{18d}$$

$$\text{H} + \text{H} \rightleftharpoons \text{H}^+ + \text{H} + \text{e}, \tag{18e}$$

$$\text{H} + \text{e} \rightleftharpoons \text{H}^+ + \text{e} + \text{e}. \tag{18f}$$

The initial ionization of hydrogen molecules by a strong shock wave was studied by Belozerov & Measures (1969). From a comparison of theoretical and experimental results, they determined the excitation cross-section constant for hydrogen atom–atom collisions to be $3{\cdot}57 \times 10^{-18}$ cm^2/eV, which is about $\frac{1}{15}$ of that of the corresponding cross-section constant for electron–atom excitational collisions. The excitation cross-section constants for collisions between argon and hydrogen atoms are difficult to determine. However, the method used by Kelly (1966) in his treatment of the argon–xenon case was adopted herein.

3. Experimental equipment and methods

The UTIAS combustion-driven 10×18 cm Hypervelocity Shock Tube, equipped with a Mach–Zehnder interferometer with a field of view 23 cm in diameter, was used for the experiments. The interferometer had a pulsed (30 ns) ruby laser light source capable of taking two simultaneous interferograms at 3471·5Å and 6943Å. From these it was possible to determine the electron number density and total density throughout the flow (see Bristow & Glass 1972; Brimelow 1974).

The tube was pumped down to 10^{-5} torr at an outgassing rate of about 10^{-5} torr/min. The argon test gas used had a purity better than 99·996% by volume. It was introduced into the driven section immediately before an experiment, and the pressure was monitored by a Wallace–Tiernan gauge and a sensitive oil manometer (0–50 torr range). In each experiment the initial pressure of the test gas was nominally 5 torr.

Measurements of shock velocity were obtained between a reference station and four positions along the tube using standard piezoelectric pressure transducers, whose outputs were amplified before being applied to two Hewlett–Packard (type 3734A) and two Racal electronic counters, measuring in μs units. A fifth velocity measurement was taken across the 61 cm of the test-section using a Hewlett–Packard (type 5325A) counter measuring in 0·1 μs units. A Kistler (601B) pressure transducer was used to record the pressure through the shock wave and the subsequent flow.

Figure 1 (plate 1) consists of interferograms taken at 6943Å and 3472Å and illustrates the passage of shock waves at a shock Mach number $M_s = 14{\cdot}7$ in argon at an initial pressure $p_0 = 4{\cdot}08$ torr, an initial temperature $T_0 = 297{\cdot}8$ °K, a degree of ionization $\alpha = 10{\cdot}6\,\%$ and $n_{e,E} \sim 10^{17}/\text{cm}^3$ with an air-impurity level of 0·0055%. The shock wave is moving from right to left. Clearly visible are the sinusoidal-type oscillations of the translational-shock front S, where the fringes change abruptly, followed by a relaxation length of 4·4 cm terminating in the electron-cascade front E, which is followed by disturbances in the fringes at this front and beyond into the quasi-equilibrium region. The approach of the electron front to the translational shock wave towards the wall is also well illustrated, especially at the higher wavelength, which is more sensitive to electrons, thereby producing a larger fringe shift.

Figure 2 (plate 2) illustrates the effects of adding hydrogen to the argon in quantities of from 0·033% H_2 to 1·0% of H_2. All interferograms were taken at 6943 Å at nominal values $M_s \sim 17$, $p_0 \sim 3$ torr, $T_0 \sim 300$ °K, $\alpha \sim 18\,\%$ and $n_e \sim 1{\cdot}4 \times 10^{17}/\text{cm}^3$. The

---

FIGURE 1. Shock structure in ionizing argon. The shock wave is moving from right to left in the UTIAS 10×18 cm Hypervelocity Shock Tube. The sharp rise in fringe shift across the wavy translational shock front is readily seen. It is followed by a gently decreasing fringe shift as electrons are produced by atom–atom collisions and then by a very sudden decrease in fringe shift due to the electron cascade formed by electron–atom impact. The fringes then rise gradually again as the electron number density is decreased owing to radiation. Instabilities in the cascade front and downstream of it are also seen. Note how this front approaches the translational shock wave as it moves closer to the wall for the longer wavelength, which is more sensitive to electrons. $p_0 = 4{\cdot}08$ torr (0·0055% air impurity), $T_0 = 297{\cdot}8$ °K, $\rho_0 = 8{\cdot}80 \times 10^{-6}$ g/cm^3, $a_0 = 321{\cdot}37$ m/s, $M_s = 14{\cdot}7$, $\alpha = 10{\cdot}6\,\%$, $M_E = 2{\cdot}22$, $n_{e,E} = 9{\cdot}57 \times 10^{16}$ cm^3, $u_E = 4031{\cdot}4$ m/s, $T_F = 20380$ °K, $T_E = 12200$ °K, $p_E = 1261$ torr, $\rho_E = 6{\cdot}00 \times 10^{-5}$ g/cm^3, $x_E \sim 4{\cdot}4$ cm, $\lambda_1 = 6943$Å, S = translational shock front, E = electron cascade, F = frozen, E = equilibrium.

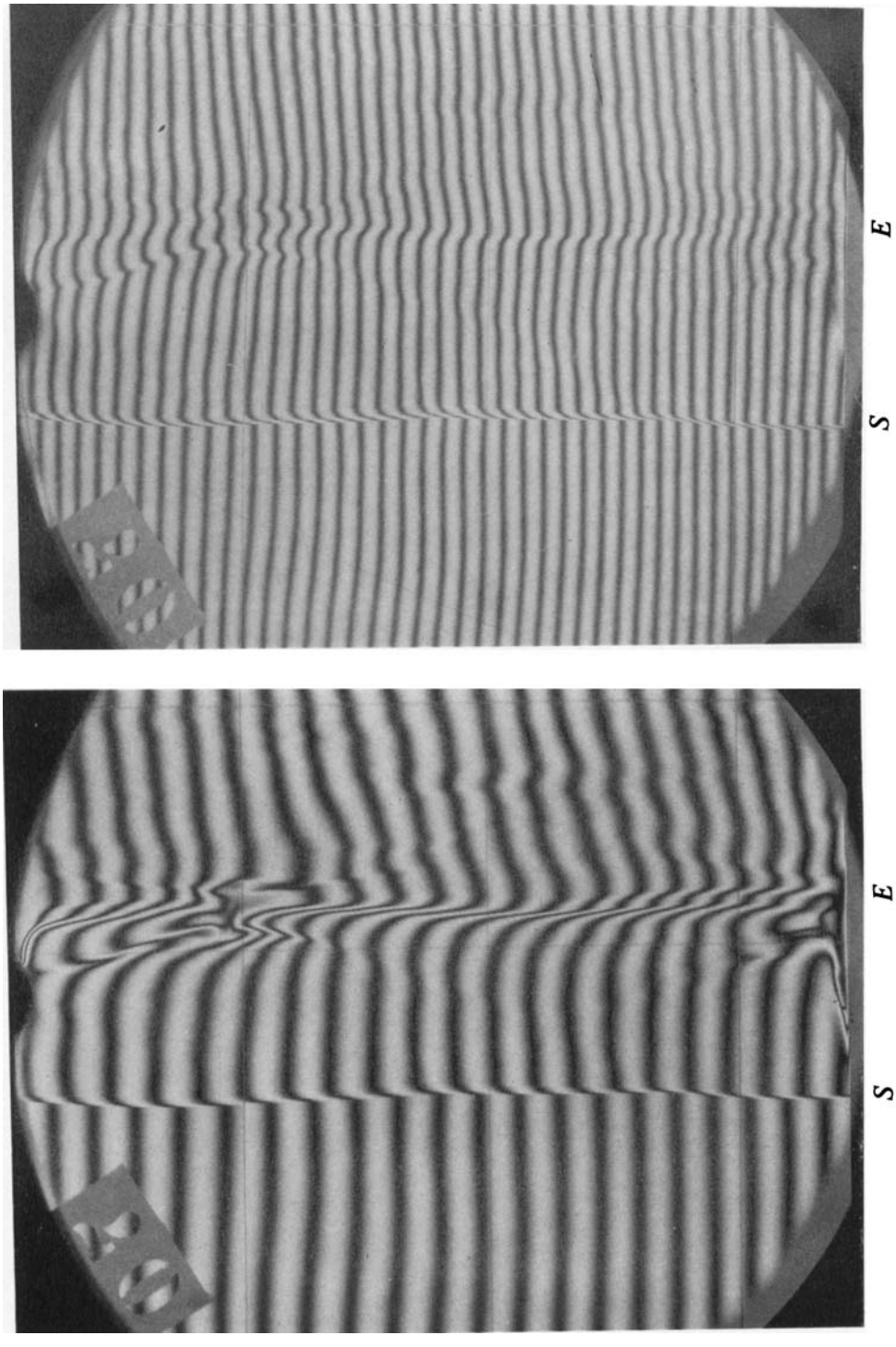

FIGURE 1. For legend see facing page.

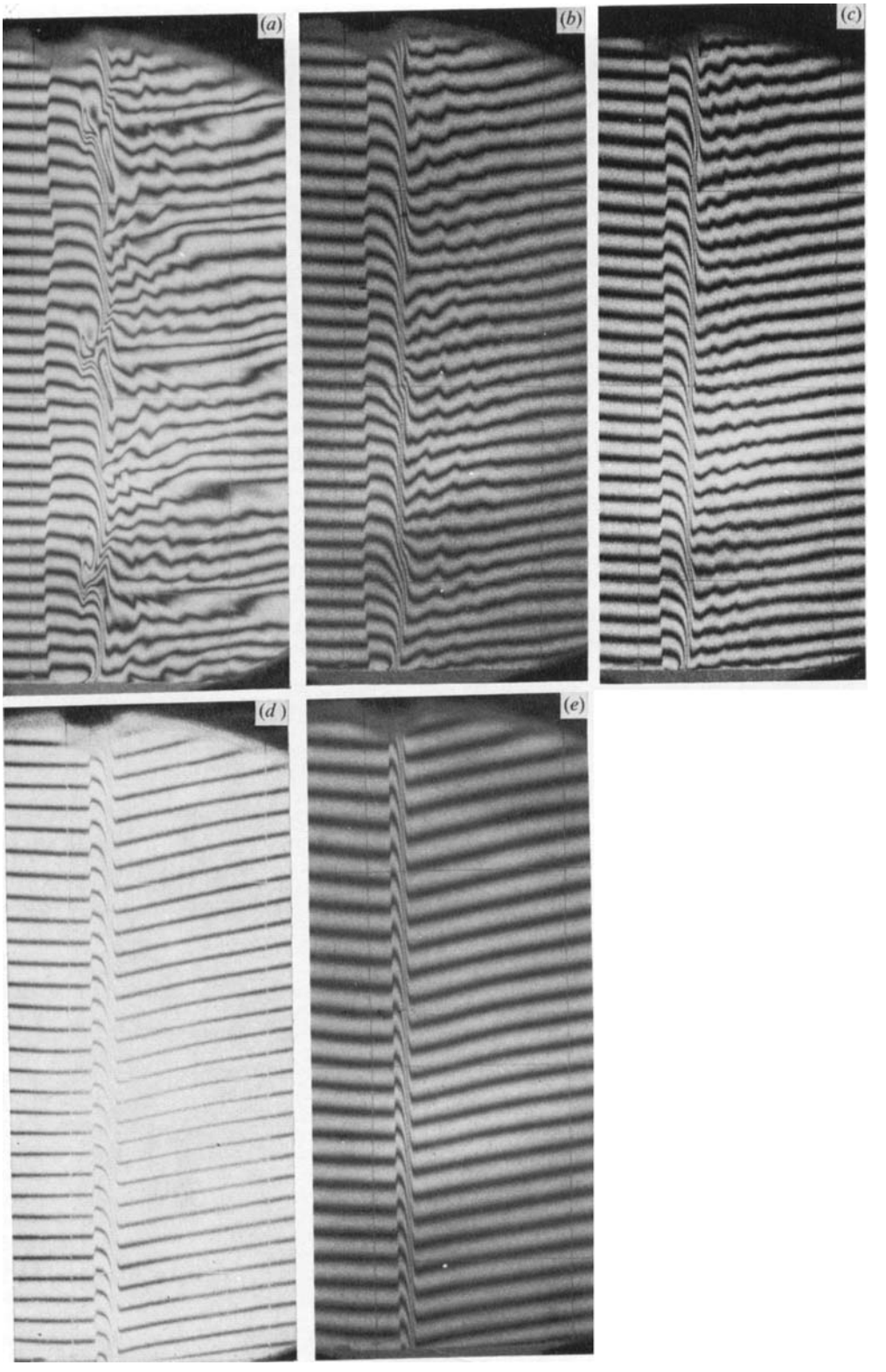

FIGURE 2. For legend see facing page.

dramatic attainment of shock-wave stability and the reduction in the relaxation length to about one-third (0·5 cm) of the pure-argon value can be easily seen.

Figure 3 (plate 3) shows that (*a*) oxygen and (*b*) helium have no noticeable effects on the argon shock-wave stability or structure. It also illustrates that the fringes in pure nitrogen (*c*), at a similarly high shock Mach number, behave in the classical manner, i.e. they are straight in the initial and final states and their approach to dissociation equilibrium is exponential.

An example of a weaker shock wave in argon at

$$M_s = 13{\cdot}0, \quad p_0 = 5{\cdot}01 \text{ torr}, \quad T_0 = 296{\cdot}8\ ^\circ\text{K}, \quad \alpha = 6{\cdot}0\,\%, \quad n_e = 5{\cdot}6 \times 10^{16}/\text{cm}^3$$

appears in figure 4 (plate 4). A lack of oscillations and a long relaxation length (8·9 cm) are strikingly evident. It is therefore apparent that the coupled oscillations noted in figures 1–3 are due to significant ionization in argon.

In order to obtain the argon–argon collisional excitation cross-section $S^*_{\text{Ar Ar}}$ and then to study the effects of hydrogen impurity a number of experiments were conducted. A few representative cases are listed in table 1. Additional experiments can be found in Bristow & Glass (1972), Brimelow (1974), Whitten (1977) and Tang (1977).

Measurements of the fringe shift through the Rankine–Hugoniot translational shock front were taken from the interferograms of the experiments. Owing to the very high density gradient through the front and the instabilities giving a possible three-dimensional effect along the light path it appears very much thicker than is really the case. The measurements of the fringe shift (i.e. the displacement of a fringe between the undisturbed gas region and the reasonably uniform flow region behind the front) were substituted into the interferometric equations for ρ and n_e as follows:

$$\rho_j = \rho_i - \frac{\lambda_1 c_2 S_1}{KL} + \frac{\lambda_2 c_1 S_2}{KL}, \tag{19}$$

$$n_{ej} = n_{ei} - \frac{\lambda_1 K_{A2} S_1}{m_a KL} + \frac{\lambda_2 K_{A1} S_2}{m_a KL}, \tag{20}$$

where L is the test-section width ($L = 10{\cdot}16$ cm), K_{A1} and K_{A2} are the Gladstone–Dale constants for argon atoms, ρ is the density, S is the non-dimensional fringe shift, n_e is the electron number density, c and K are given by

$$c_1 = 0{\cdot}33\,K_{A1} + 0{\cdot}67 \times 10^9 \lambda_1^2,$$

$$c_2 = 0{\cdot}33\,K_{A2} + 0{\cdot}67 \times 10^9 \lambda_2^2,$$

$$K = c_1 K_{A2} - c_2 K_{A1},$$

λ is the wavelength, i denotes a reference value while j denotes an unknown value. For the light-source wavelengths used in the present experiments

$$(\lambda_1 = 6943\text{Å}, \quad \lambda_2 = 3471{\cdot}5\text{Å})$$

FIGURE 2. Shock structure in ionizing argon with H_2 impurities. (*a*) $p_0 = 2{\cdot}84$ torr (0·033 % H_2), $T_0 = 296{\cdot}8$ °K, $M_s = 17{\cdot}0$, $\alpha = 18{\cdot}0\,\%$, $n_{e,E} = 1{\cdot}38 \times 10^{17}/\text{cm}^3$. (*b*) $p_0 = 2{\cdot}98$ torr (0·1 % H_2), $T_0 = 297{\cdot}6$ °K, $M_s = 17{\cdot}0$, $\alpha = 18{\cdot}0\,\%$, $n_{e,E} = 1{\cdot}44 \times 10^{17}/\text{cm}^3$. (*c*) $p_0 = 2{\cdot}85$ torr (0·2 % H_2), $T_0 = 298{\cdot}0$ °K, $M_s = 17{\cdot}1$, $\alpha = 18{\cdot}4\,\%$, $n_{e,E} = 1{\cdot}41 \times 10^{17}/\text{cm}^3$. (*d*) $p_0 = 2{\cdot}88$ torr (0·5 % H_2), $T_0 = 295{\cdot}7$ °K, $M_s = 17{\cdot}2$, $\alpha = 18{\cdot}4\,\%$, $n_{e,E} = 1{\cdot}44 \times 10^{17}/\text{cm}^3$. (*e*) $p_0 = 2{\cdot}85$ torr (1·0 % H_2), $T_0 = 294{\cdot}8$ °K, $M_s = 17{\cdot}3$, $\alpha = 18{\cdot}8\,\%$, $n_{e,E} = 1{\cdot}48 \times 10^{17}/\text{cm}^3$.

Interferograms from references	Cases analysed	p_0(torr)	M_s	T_0(°K)	Gases
Tang (1977)	1	5.14	15·9	293·6	Argon
Tang (1977)	2	5·15	16·1	295·9	Argon
Brimelow (1974)	3	5·12	16·5	296·6	Argon
Whitten (1977); see figure 5(*a*)	4	5·01	13·0	296·6	Argon
Brimelow (1974)	5	5·17	16·2	297·0	Ar + 0·4 % H_2
Tang (1977)	6	3·12	17·7	298·2	Ar + 0·4 % H_2

TABLE 1. Initial conditions for the cases studied.

the constants take on values of $K_{A1} = 0{\cdot}1572$ cm^3/g, $K_{A2} = 0{\cdot}1627$ cm^3/g, $c_1 = 3{\cdot}2816$ cm^3/g, $c_2 = 0{\cdot}8611$ cm^3/g and $K = 0{\cdot}3986$ cm^6/g^2; the degree of ionization $\alpha = n_e/(n_a + n_e)$ or $\alpha = m_a n_e/\rho$ (see Tang 1977).

4. Results and discussion

General description of interferograms and errors

The interferograms shown in figures 1–4 illustrate very well the structure of ionizing shock waves. The Rankine–Hugoniot front is evident as a sudden, almost discontinuous shift in the fringes. Behind this front, changes in the flow properties take place very slowly as the gas begins to relax through atom–atom collisions (this shows up as a region in which the fringes shift downwards very slowly). As more and more electrons are formed they become very effective collision partners so a rapid cascading of electrons occurs and the fringes drop suddenly.

It may be noted that while the non-dimensional fringe shift through the Rankine–Hugoniot front is about 0·75 for λ_2 and 1·5 for λ_1 for a maximum density ratio of about 4 for a perfect gas, the shifts through the ionization front are much larger (5·5 for λ_1 and 2 for λ_2) even though the increase in the density ratio is only about 2. This is due to the negative contribution by the electrons to the refractive index. Since this effect is more sensitive to the longer wavelength, such interferograms are much more striking in appearance.

If an error equation (Tuttle & Satterly 1925, p. 231) is applied to the interferometric equations (19) and (20) for a fringe-shift error of 0·05–0.08, the error is about 3×10^{-6} g/cm^3 in ρ and 5×10^{15} cm^{-3} in n_e. These errors are uniform over the entire flow. The error in α depends on both ρ and n_e at different locations and is usually about 0·4 % or less. Consequently, for a given initial pressure, as the Mach number, density and electron number density decrease the percentage error in ρ and n_e will become progressively greater.

The errors for the measured pressure and Mach number are about 0·5 % and 2 %, respectively. Although shock Mach numbers are measured over several stations of the 14·6 m channel, it is the final Mach number measured over a 61 cm length along the test section that is used. It should be noted that the effects of an error in the measured Mach number on the shock structure are more significant than that of an error in the measured pressure.

Free-stream relaxation region

From figure 1, let the distance between the shock S and the point of maximum electron number density E be the relaxation length x_E, measured from the shock S. For a fixed shock Mach number M_s and an initial pressure p_0, the value of this length calculated from the theoretical model depends on: the excitational cross-section constants S^*_{aa} and S^*_{ea} for atom–atom and electron–atom collisions, respectively; the momentum transfer cross-sections $Q_{ea}(T_e)$ and $Q_{ei}(T_e, n_e)$ for electron–atom and electron–ion collisions, respectively; and the total radiation loss Q_R. That is,

$$x_{E\text{th}} = x_E(S^*_{aa}, S^*_{ea}, Q_{ea}, Q_{ei}, Q_R).$$

A study of their relative effect shows that increasing either S^*_{aa} or $Q_{ei}(T_e, n_e)$ by a factor of two causes a 20 % decrease in the calculated value of x_E, while doubling S^*_{ea} or $Q_{ea}(T_e)$ gives only a 10 % decrease. The inclusion of the radiation loss term Q_R yields a definite position where the electron number density reaches a maximum (verified experimentally) rather than a somewhat arbitrary position without radiation where the approach to a constant equilibrium value is asymptotic. Other than this, however, the choice of the radiation model has little or no effect on the calculated value of x_E. However, it plays the major role in providing for the correct variation of n_e and ρ in the quasi-equilibrium region.

As mentioned previously, the more recent value of $S^*_{e\,\text{Ar}} = 4{\cdot}9 \times 10^{-18}$ cm^2/eV (Zapesochnyi & Felston 1966) is used in the calculations, although using the earlier value $S^*_{e\,\text{Ar}} = 7{\cdot}0 \times 10^{-18}$ cm^2/eV (see Petschek & Byron 1957) has only a 5 % effect on x_E. The variation of Q_{ea} with temperature calculated by Devoto (1967) is assumed as the best available to date. Similarly, the relationship for $Q_{ei}(n_e, T_e)$ from a classical Coulomb scattering model should be accurate to within a factor less than 1·5. Therefore the calculated value of x_E remains a sensitive function of $S^*_{\text{Ar Ar}}$, whose previously determined values have varied by an order of magnitude or more. In summary, it can be stated that the value of $S^*_{\text{Ar Ar}}$ determined here, which was obtained from a fit of the experimental data from S to x_E, is considered more reliable than obtained previously. That is, the theoretical curve was made to fit the centre-point (0·5) of $n_e/n_{e,E}$ and the relaxation distance x_E, which assured the best agreement with the interferometric data at the initial and final points of the n_e plot.

The initial conditions of the cases analysed are given in table 1. It was decided to use the $M_s \sim 16$ and $p_0 \sim 5$ torr data as the model case. A number of values of $S^*_{\text{Ar Ar}}$ were used in the numerical analysis as a best fit to the measured interferometric shock transition over the relaxation length x_E. From the best fit the value for the argon–argon excitational collision cross-section constant is obtained. If a possible error in the experimental Mach number (~ 2 %) is included in the analysis the best value of $S^*_{\text{Ar Ar}}$ becomes $(1{\cdot}0 \pm 0{\cdot}1) \times 10^{-19}$ cm^2/eV. However, in view of the unknowns in the values of the cross-sections, the deviation is not justified. The calculated and measured values of x_E are shown in table 2 for comparison. In all cases $S^*_{\text{Ar Ar}} = 1{\cdot}0 \times 10^{-19}$ cm^2/eV was used. It is seen that poor agreement results for case 4, $M_s = 13{\cdot}0$ and $p_0 = 5{\cdot}01$ torr. A value of $S^*_{\text{Ar Ar}} = 2 \times 10^{-19}$ cm^2/eV would give a much better fit to the interferometric data. It is not clear why $S^*_{\text{Ar Ar}}$ should be larger at the lower M_s.

The equilibrium (real gas without radiation losses) density ρ_E, electron number

Cases	Theory (cm)	Experiment (cm)
1	2·10	2·00
2	2·00	1·90
3	1·75	1·80
4	10·9	8·90
5	0·77	0·65
6	0·80	0·75

TABLE 2. Comparison of calculated and experimental relaxation lengths x_E using $S^*_{\mathrm{Ar\,Ar}} = 1{\cdot}0 \times 10^{-19}$ cm^2/eV.

Cases	ρ_E(g/cm^3)	$n_{e,E}$(cm^{-3})	α_E
1	$0{\cdot}84 \times 10^{-4}$	$1{\cdot}69 \times 10^{17}$	0·14
2	$0{\cdot}87 \times 10^{-4}$	$1{\cdot}83 \times 10^{17}$	0·15
3	$0{\cdot}88 \times 10^{-4}$	$2{\cdot}10 \times 10^{17}$	0·16
4	$0{\cdot}62 \times 10^{-4}$	$5{\cdot}62 \times 10^{16}$	0·06
5	$0{\cdot}82 \times 10^{-4}$	$1{\cdot}94 \times 10^{17}$	0·15
6	$0{\cdot}56 \times 10^{-4}$	$1{\cdot}83 \times 10^{17}$	0·21

TABLE 3. Thermal equilibrium values of the density ρ_E, electron number density $n_{e,E}$ and degree of ionization α_E without radiation losses ($Q_R = 0$).

density n_{eE} and degree of ionization α_E are listed in table 3. The transition properties for pure argon (cases 1–4) are shown in figures 5–8. Figure 5 (*a*) (case 1) shows a plot of the non-dimensional electron number density $n_e/n_{e,E}$ through the shock-wave transition and beyond, as well as the non-dimensional density ratio ρ/ρ_E, including the error bars. The measured shock Mach number was $M_s = 15{\cdot}9$ (solid curves). The position $x = 0$ is where the translational shock wave is located (S in figure 1). The position x_E (or E in figure 1) denotes the electron cascade front or the end of the transition region. Here the flow quantities achieve their maximum equilibrium values (subscript E). In this region the radiation losses $Q_R \sim 0$. Beyond this point, since $Q_R \neq 0$, the electron number density falls. Consequently, the density continues to rise. Without radiation losses $n_e/n_{e,E}$ and ρ/ρ_E would approach unity. However, since radiation losses were included, these quantities are theoretically less than unity.

To estimate the effects of a possible error in the Mach number of $\pm 0{\cdot}3$, two additional curves are plotted for $M_s = 16{\cdot}2$ (dashed) and 15·6 (dot–dash). Furthermore, to obtain a best fit to the interferometric data the corresponding values of $S^*_{\mathrm{Ar\,Ar}}$ were changed to $0{\cdot}9 \times 10^{-19}$ cm^2/eV and $1{\cdot}1 \times 10^{-19}$ cm^2/eV, respectively. It is seen that the greatest effect is on the post-shock quasi-equilibrium region as expected. Since the same value of x_E was used in all three cases, the lines should be superimposed from 0 to x_E, but were separated for clarity. It should also be noted that, since the values of ρ_E and $n_{e,E}$ for $M_s = 15{\cdot}9$ are used for normalizing, then for $x = x_E$ at $M_s = 15{\cdot}9$, $n_e/n_{e,E} \to 1$, for $x = x_E$ at $M_s = 15{\cdot}6$, $n_e/n_{e,E} < 1$ and for $x = x_E$ at $M_s = 16{\cdot}2$, $n_e/n_{e,E} > 1$. The value of x_E noted on the graphs is the theoretical value when $n_e = n_{e,E}$ is a maximum and differs from the experimental value by ~ 1 mm. The interferometric data points were taken 1 mm apart in the most quiescent parts of the interferograms to avoid oscillations. More or fewer points can be measured depending on the work and type of data required.

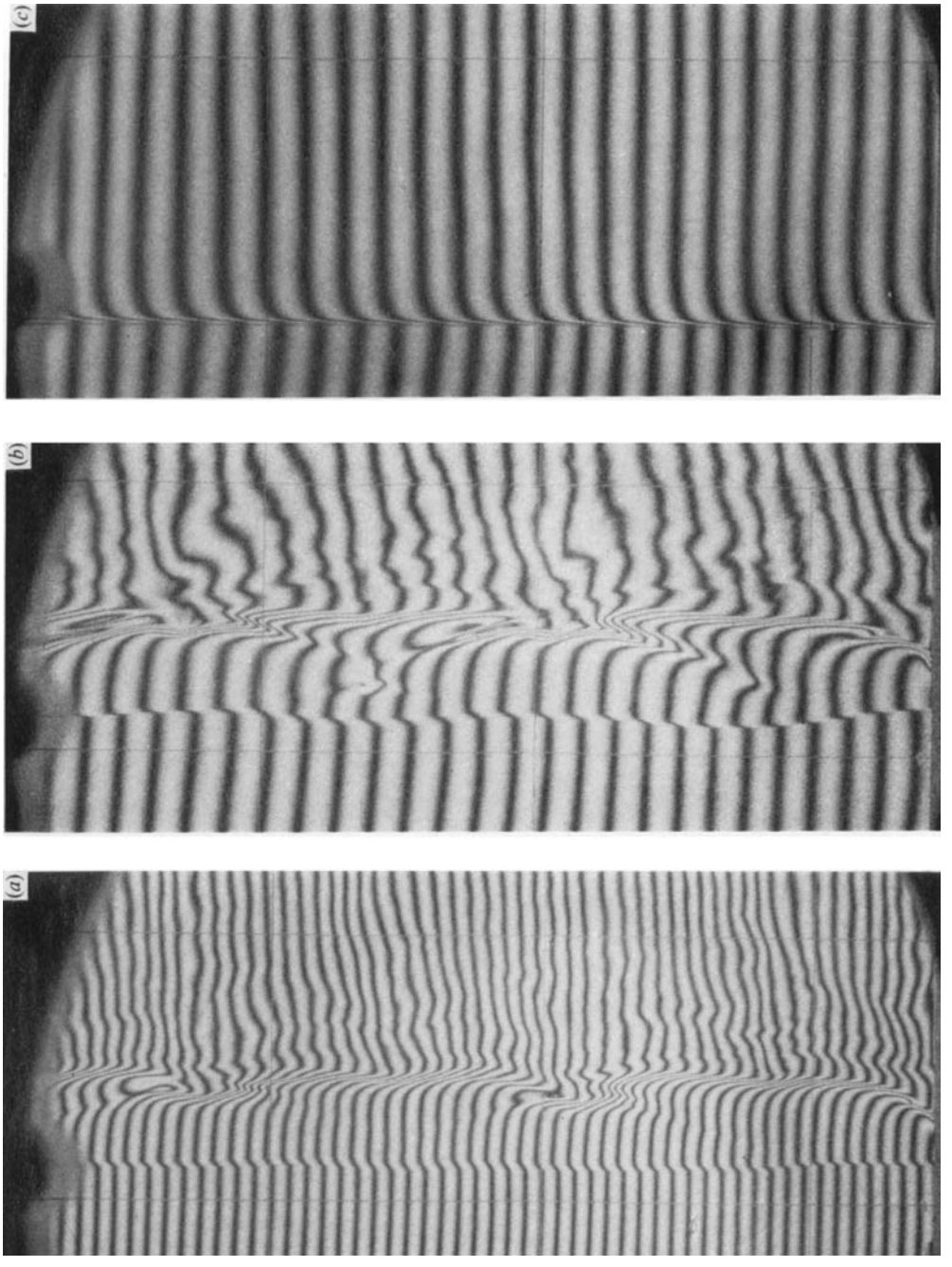

FIGURE 3. Shock structure in ionizing argon. (*a*) Impurity O_2 (0·46 %), $p_0 = 2{\cdot}85$ torr, $T_0 = 295{\cdot}7$ °K, $M_s = 17{\cdot}1$, $\alpha = 17{\cdot}9$ %. (*b*) Impurity He (1·08 %), $p_0 = 2{\cdot}87$ torr, $T_0 = 295{\cdot}6$ °K, $M_s = 17{\cdot}1$, $\alpha = 18{\cdot}4$ %. (*c*) Pure N_2, $p_0 = 2{\cdot}03$ torr, $T_0 = 296{\cdot}0$ °K, $M_s = 16{\cdot}6$, dissociation fraction = 30 %.

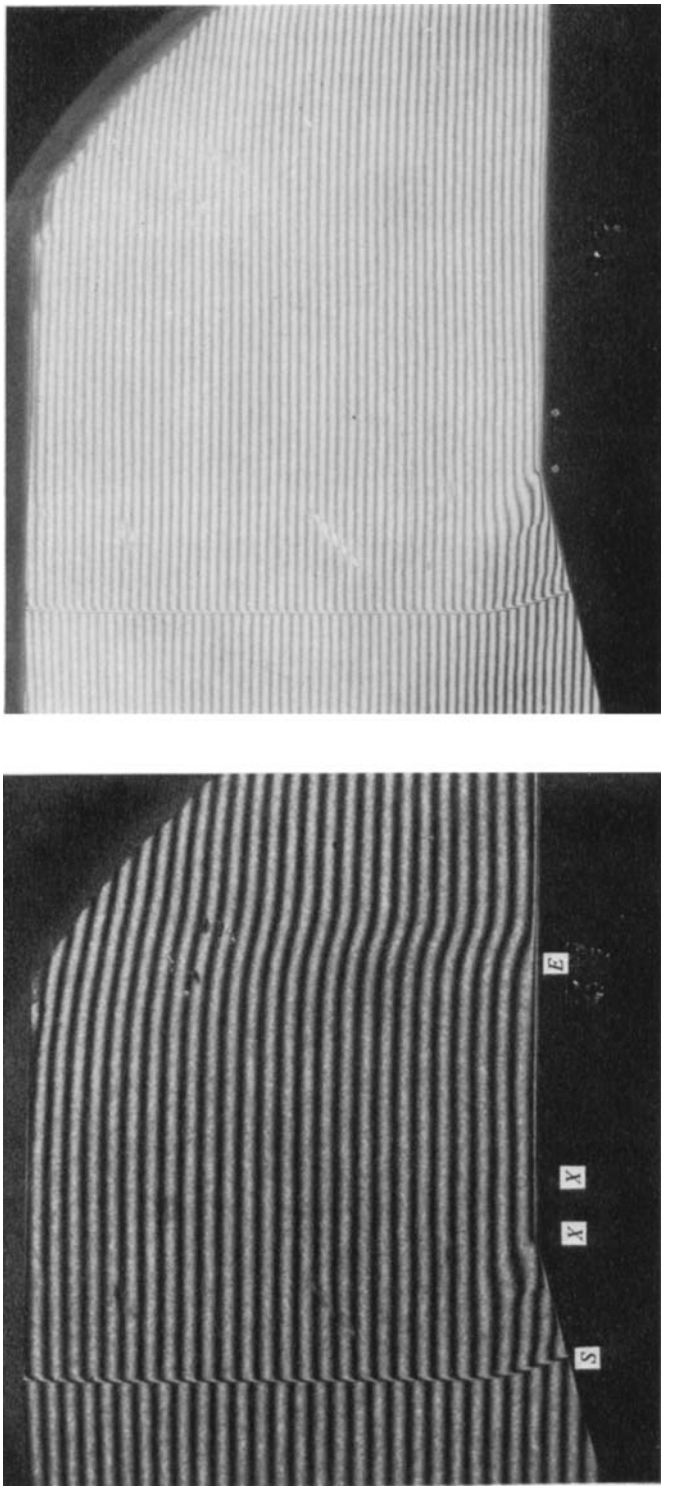

FIGURE 4. Diffraction of a shock wave around a 15° sharp corner in ionizing argon. A quasi-steady interaction of the expansion wave with the boundary layer results. $M_s = 13{\cdot}0$, $p_0 = 5{\cdot}01$ torr, $\rho = 1{\cdot}08 \times 10^{-5}$ g/cm^3, $T_0 = 296{\cdot}8$ °K, $a_0 = 320{\cdot}8$ m/s, $\alpha = 6\,\%$, $n_{a\,E} = 5{\cdot}62 \times 10^{16}$/cm^3, $n_{a,E} = 8{\cdot}80 \times 10^{17}$/cm^3, $T_E = 11\,400$ °K, $a_E = 1732$ m/s, $\rho_E = 6{\cdot}21 \times 10^{-5}$ g/cm^3, $p_E = 1172$ torr, $M_E = 1{\cdot}98$, $\lambda_1 = 6943$Å, $\lambda_2 = 3471$Å, $x_E \sim 8{\cdot}9$ cm, X–$X = 1{\cdot}0$ cm (between reference cross-wires), S = translational shock wave, E = electron-cascade front.

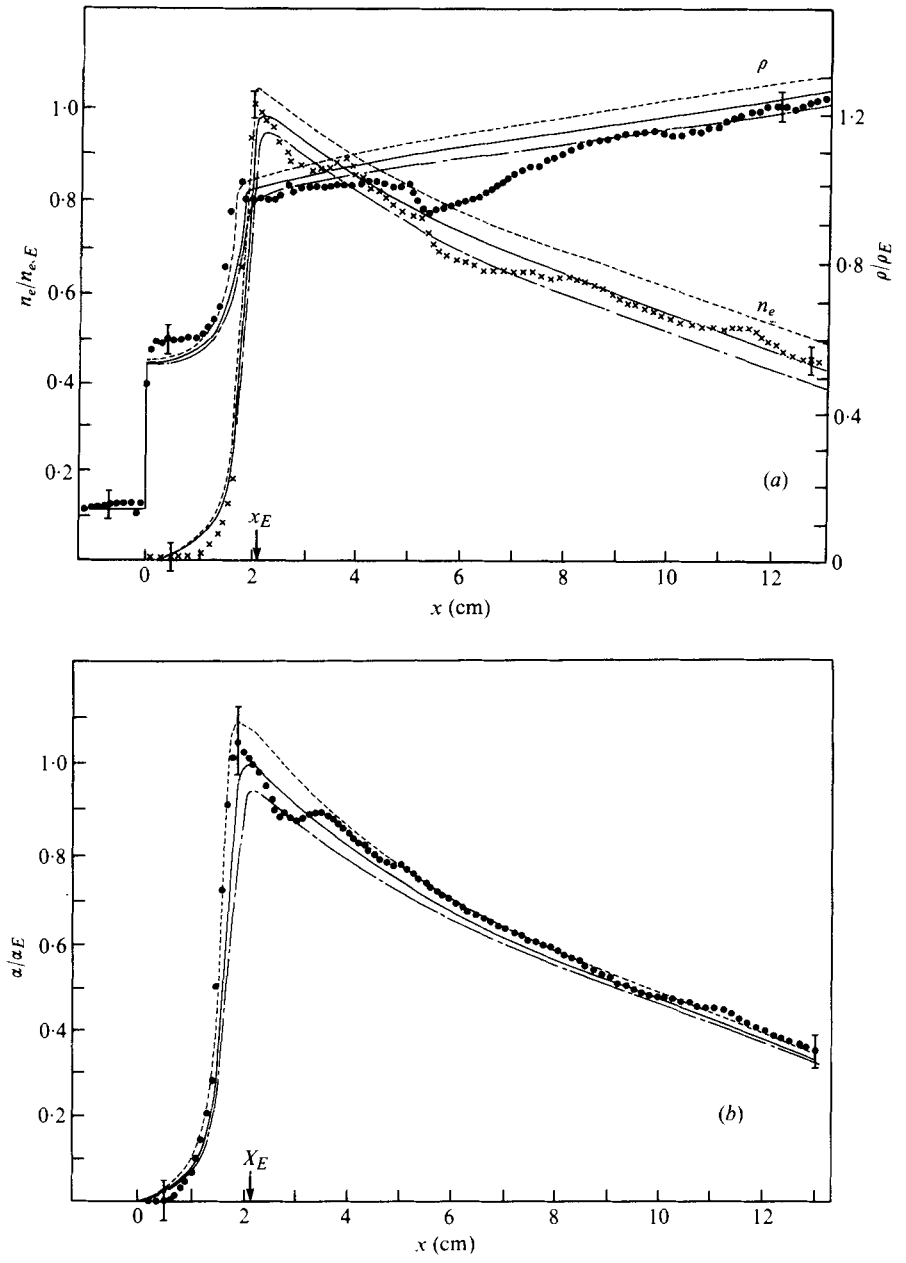

FIGURE 5. Variation of (*a*) the density ρ and electron number density n_e and (*b*) the degree of ionization α with distance x for case 1: $p_0 = 5{\cdot}14$ torr, $T_0 = 293{\cdot}6$ °K. ---, $M_s = 16{\cdot}2$, $S^*_{\mathrm{Ar\,Ar}} = 0{\cdot}9 \times 10^{-19}$ cm²/eV; ——, $M_s = 15{\cdot}9$, $S^*_{\mathrm{Ar\,Ar}} = 1{\cdot}0 \times 10^{-19}$ cm³/eV; -·-, $M_s = 15{\cdot}6$, $S^*_{\mathrm{Ar\,Ar}} = 1{\cdot}1 \times 10^{-19}$ cm²/eV.

The fit to the experimental data is quite reasonable. The measured n_e values are lower than those predicted by the analysis during the initial part of the transition and the density is therefore higher. The post-shock n_e is oscillatory but in good agreement with the analysis, lending support to the estimates of the radiation losses Q_R, but the density is not in such good agreement. The oscillations of the fringes in the pure-argon

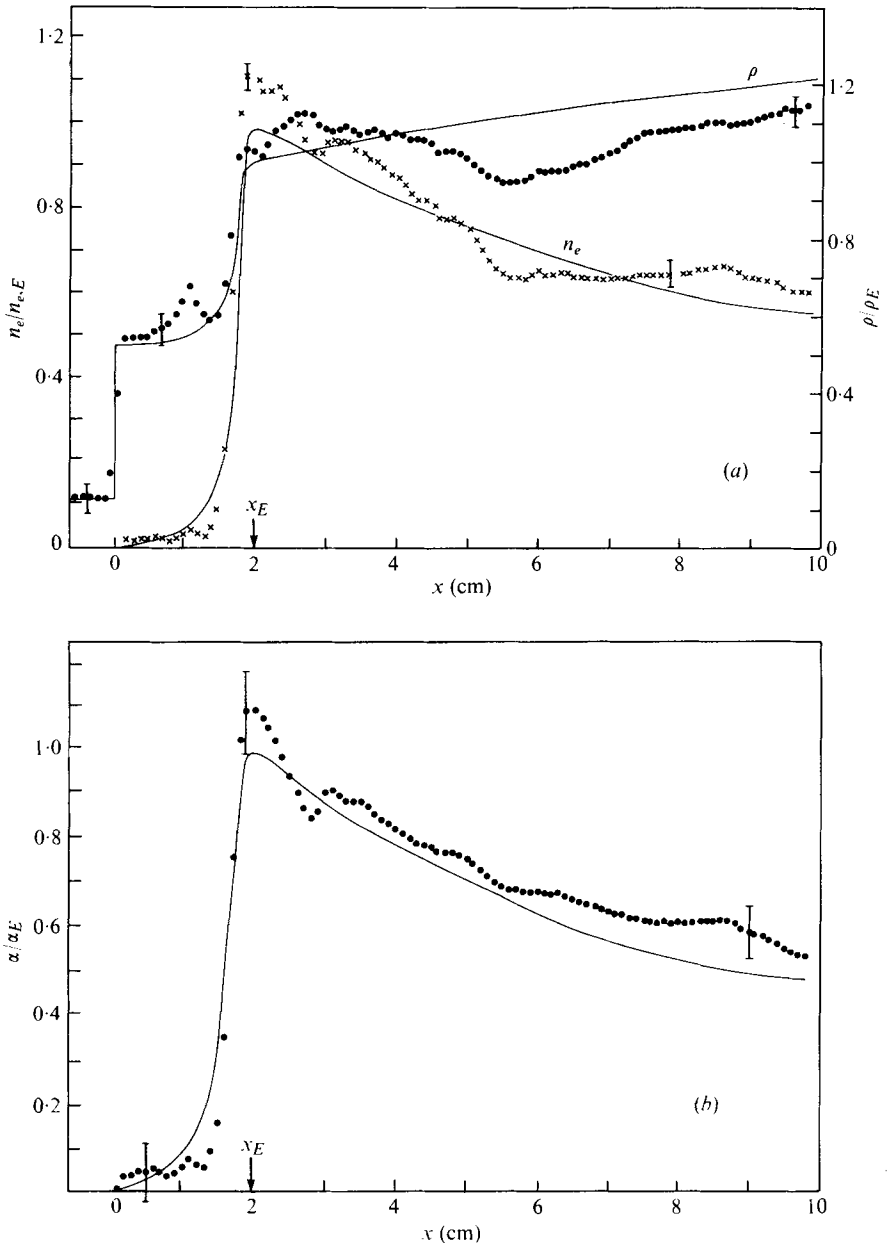

FIGURE 6. Variation of (*a*) ρ and n_e and (*b*) α with x in argon for case 2: $p_0 = 5{\cdot}15$ torr, $T_0 = 295{\cdot}9$ °K, $M_s = 16{\cdot}1$.

case in the quasi-equilibrium region are reflected in the oscillations of n_e and ρ. The relaxation length obtained from the experimental results is about 2·0 cm if the n_e plot is used and about 1·6 cm for the ρ plot. However, the latter does not define x_E very accurately.

Figure 5 (*b*) shows a plot of the degree of ionization α *vs.* the distance x. It is really a

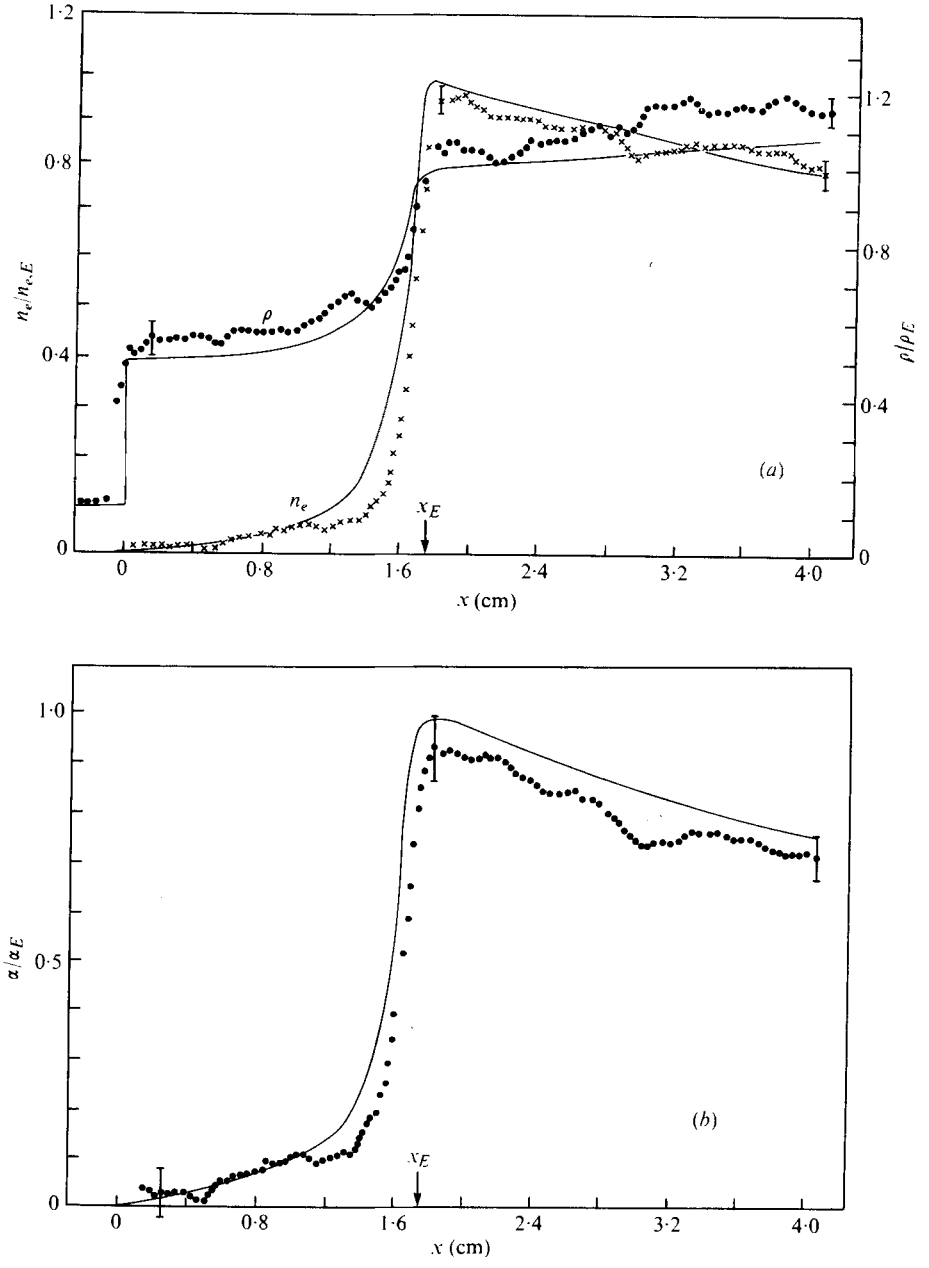

FIGURE 7. Variation of (*a*) ρ and n_e and (*b*) α with x in argon for case 3: $p_0 = 5{\cdot}12$ torr, $T_0 = 296{\cdot}6$ °K, $M_s = 16{\cdot}5$.

reflexion of n_e *vs.* x. The post-shock values after 3 cm are in particularly good agreement with the analysis. The effects of radiation-energy losses or radiative cooling are evident from the decrease in the degree of ionization, as described by Oettinger & Bershader (1967).

Similar comments apply to case 2 (figure 6) and case 3 (figure 7). However, although the experimental results for higher Mach numbers ($\sim$ 16) are in fair to good agreement

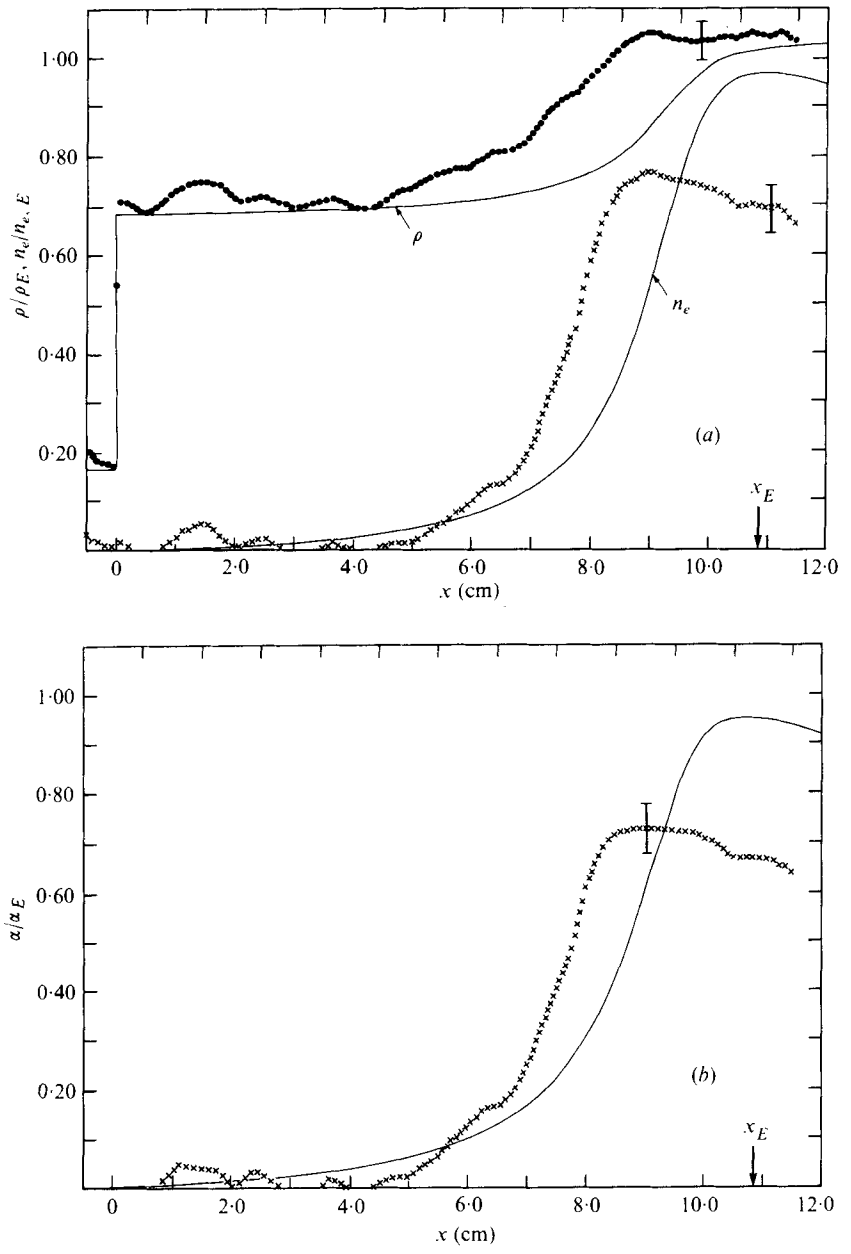

FIGURE 8. Variation of (*a*) ρ and n_e and (*b*) α with x in argon for case 4: $p_0 = 5{\cdot}0$ torr, $T_0 = 296{\cdot}6$ °K, $M_s = 13{\cdot}0$.

with the analysis, for lower Mach numbers ($M \sim 13$: case 4, figure 8) the agreement is not satisfactory. As noted previously better agreement could have been obtained by using $S^*_{\mathrm{Ar\,Ar}} = 2 \times 10^{-19}\,\mathrm{cm^2/eV}$. However, this would have violated the concept that $S^*_{\mathrm{Ar\,Ar}}$ is a fixed quantity. Consequently, it may be possible that additional unknown factors are responsible for this apparent variation of $S^*_{\mathrm{Ar\,Ar}}$ as M_s, n_e and ρ are reduced and the percentage errors increase. Yet one might have assumed that the larger value

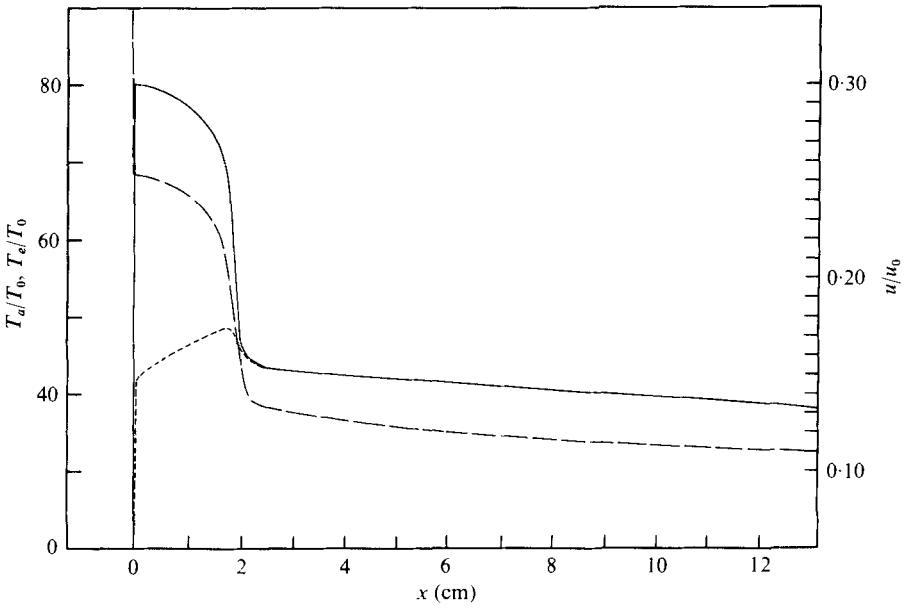

FIGURE 9. Variation of T_a, T_e and u with x for case 1.
—, T_a; - - -, T_e; – –, u.

of x_E at a lower Mach number would be beneficial for producing a better fit. These questions are worthy of further investigation.

Radiative-cooling region

The analytical variations of the particle velocity u, atom temperature T_a and electron temperature T_e for case 1 are shown in figure 9. It is seen that the particle velocity and atom temperature decrease monotonically through the transition region. The electron temperature, on the other hand, rises through the transition region to a maximum value of $T_e/T_0 \sim 49$ at $x \sim 1{\cdot}7$ cm and then falls and approaches the same value as T_a at $x \sim 2$ cm. This approach to equilibrium is more complex than the classical exponential approach to equilibrium as in the case of molecular vibration, say.

From (6) it can be seen that T_e depends on the particle velocity, the elastic energy transfer rate (the thermal energy given to the free electrons by elastic collisions with atoms and ions) and the inelastic energy transfer rate (electronic excitation of atoms). Near the shock front the electron number density is small and the inelastic energy transfer rate exceeds the elastic rate and the plasma mass kinetic energy transfer rate. The latter has little effect on the electron temperature and can be neglected (see Hoffert & Lien 1967). When the electron number density rises to a certain value (at $x \sim 0{\cdot}2$ cm), the elastic energy transfer rate increases and just exceeds the inelastic rate. At $x \sim 1{\cdot}7$ cm both reach their maximum value and then decrease slowly. At this point the electron production rate is a maximum and the inelastic transfer rate is slightly larger than the elastic rate, as deduced from the computer outputs. Therefore the electron temperature falls and blends with the atom temperature, as shown in figure 9.

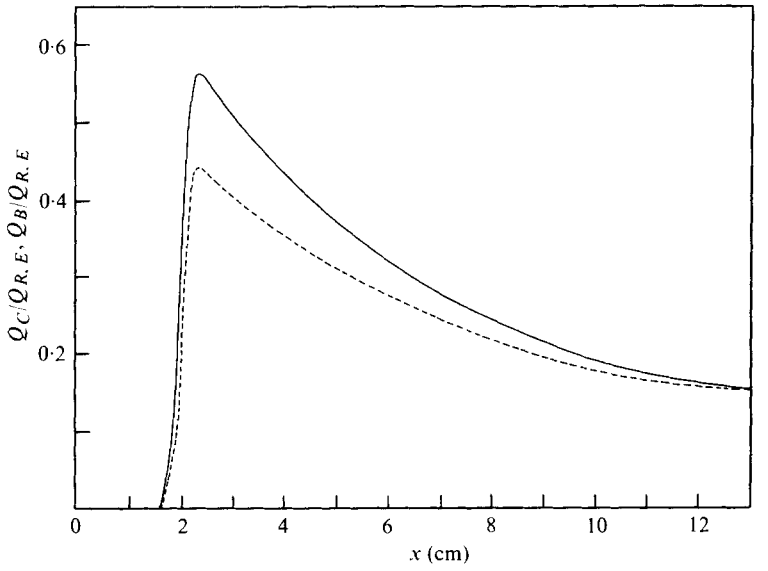

FIGURE 10. Variation of the continuum radiation energy loss Q_c due to continuum radiation and the radiation-energy loss Q_B due to line radiation with x for case 1. ——, $Q_C/Q_{R,E}$; – – –, $Q_B/Q_{R,E}$. $Q_{R,E} = 4{\cdot}52 \times 10^3$ J/cm^3 s.

It should be noted that, in the radiative-cooling region, the particle velocity, electron or atom temperatures and the electron number density all decay gradually. Consequently, their values could be calculated by using simple linear relations from any point after the relaxation distance x_E.

The ratios of the radiation-energy loss Q_C due to continuum radiation and the radiation-energy loss Q_B due to line radiation to the total radiation-energy loss Q_R at the post shock-wave equilibrium position x_E for case 1 are shown in figure 10. It is seen that the radiation-energy loss due to line radiation is somewhat smaller than that due to continuum radiation and agrees well with the results of Horn *et al.* (1967). During the initial relaxation or shock-transition thickness, the effects of radiation are negligible. The losses rise very sharply up to $x \sim 2{\cdot}3$ cm, where $Q_{R,E} = 4{\cdot}52 \times 10^3$ J/cm^3 s. Then the values decay exponentially until at $x \sim 13$ cm Q_C and Q_B are equal, and $Q_R \sim 0{\cdot}3\,Q_{R,E}$. It should be noted that these maxima are reached slightly beyond the maximum value of n_e, which occurs at $x \sim 2{\cdot}1$ cm. Since Q_C and Q_B depend on both n_e and T_e, and when n_e is a maximum T_e is still decreasing, this gives rise to a slightly larger distance of $x \sim 2{\cdot}3$ cm.

Pomerantz (1961) gave a more detailed description of the continuum radiative transfer by allowing for both re-absorption of the emitted radiation and the lowering of the ionization potential of the shocked gas by the plasma microfield, which were neglected here. However, McChesney & Al-Attar (1965) have shown that there is no significant difference between cases with or without such a correction to the ionization potential based on the equilibrium model. The solution to the set of simultaneous differential equations becomes difficult when the re-absorption energy is included, as it depends on the complete structure of the radiating zone and the shock-tube cross-section. However, since the agreement between analysis and experiment in the

radiative-cooling regions was shown to be quite good, the re-absorption energy is not significant here.

Kamimoto & Teshima (1972) have studied the electron temperature and density profiles in the radiative-cooling region in argon for lower Mach numbers ($M_s = 10{\cdot}3$ and $13{\cdot}4$) based on the equilibrium model. They assumed that the total radiation-energy loss was twice the radiation-energy loss due to continuum radiation and obtained good agreement between the calculations and experiments. Furthermore, figure 10 does substantiate that Q_C and Q_B are nearly equal.

Effects of hydrogen impurity

Calculations were made for the cases $M_s = 16{\cdot}2, p_0 = 5{\cdot}17$ torr and $M_s = 17{\cdot}7, p_0 = 3{\cdot}12$ torr (cases 5 and 6, table 1) with a small amount of hydrogen (0·4 % by pressure) as an impurity. It has already been shown in figure 2 that an impurity of this small percentage readily stabilized but shortened the entire shock transition. The resulting analytical density, electron number density and degree of ionization variations through the relaxation and radiative-cooling zones are shown in figures 11 and 12 along with the experimental data. The agreement between the predicted and measured results is fair, confirming the choice of the theoretical model. Better agreement might have been obtained by not making the assumption of equal temperatures and velocities for the heavy particles of argon and hydrogen in the theory. Improvements could also have come from using the appropriate values of the refractive indices for the hydrogen impurity in the interferometric equations (19) and (20). However, the agreement for the relaxation length and the quasi-equilibrium post-shock values is very satisfactory. The shock transition values are particularly good for the stronger shock, case 6, showing that the constant $S^*_{\mathrm{Ar\,Ar}} = 1{\cdot}0 \times 10^{-19}$ cm^2/eV is valid for higher values of M_s and lower values of p_0.

The effect of a small hydrogen impurity on the shock-wave relaxation length is quite drastic and results in a threefold reduction in this length. This result is quite different from that for the argon–xenon mixtures used by Kelly (1966). He showed that the addition of 0·1 % and 0·48 % of xenon to the argon test gas did not substantially change the relaxation length from that for pure argon. The reason is that the excitation cross-section constant for pure xenon is much smaller than that for pure argon, while the constant for pure hydrogen is significantly larger than that for argon atoms. In addition, the mass of atomic hydrogen is markedly smaller than that of the argon atom and the ionization temperature for atomic hydrogen is lower than that for argon. These three characteristics of the hydrogen impurity in the argon test gas probably account for the great reduction in the relaxation length. It is worth noting from figure 3 that neither helium nor oxygen impurities have any noticeable effect. Despite the small mass of helium, it possesses the highest ionization potential. Recent tests using water vapour as an impurity have shown results similar to those for hydrogen, as might have been expected.

An attempt was made to remove the assumption of equal velocities and temperatures for heavy particles but without success. The uncertainty of the elastic cross-sections between ions and atoms and between ions and ions for argon and hydrogen creates a difficulty in the solution of the problem. Perhaps the kinetic four-fluid model of Schultz-Grunow (1975) might overcome this difficulty.

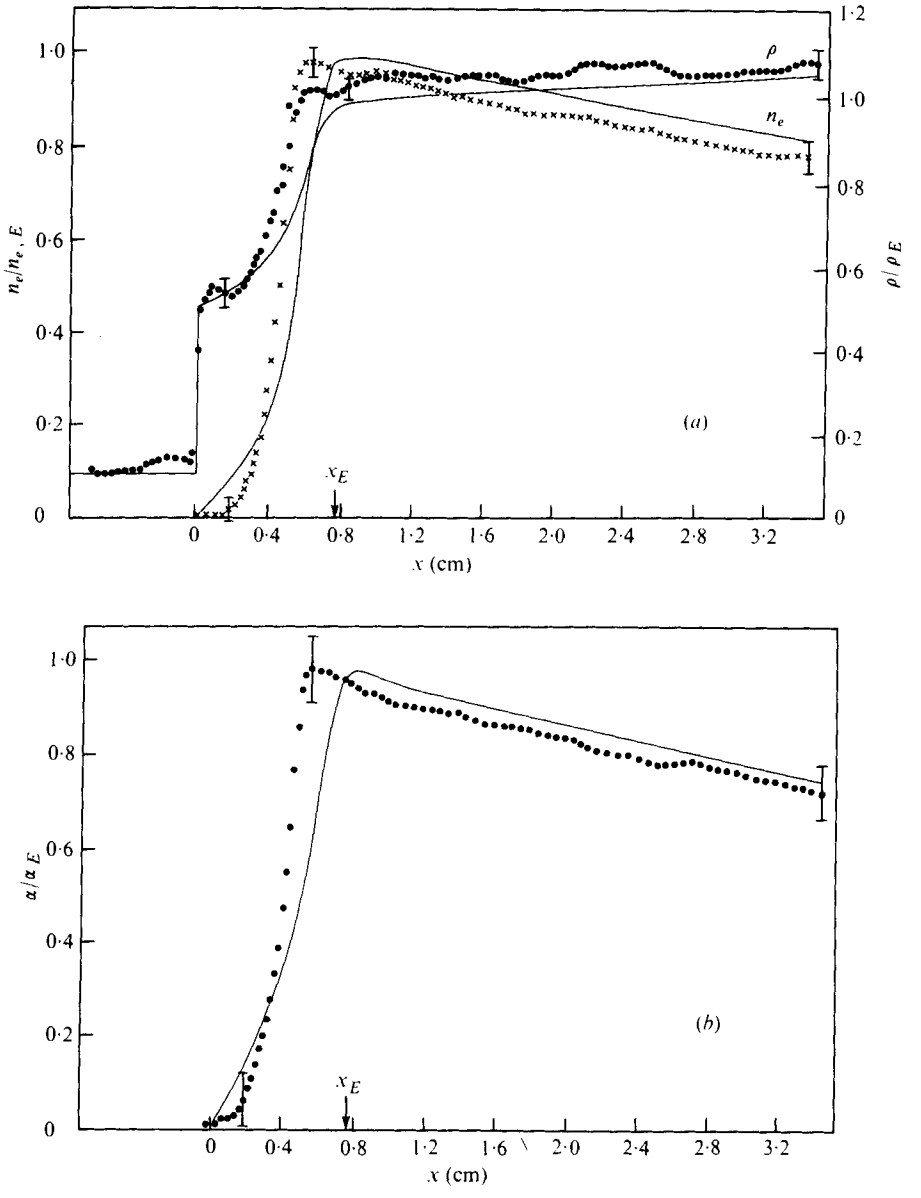

FIGURE 11. Variation of (*a*) ρ and n_e and (*b*) α with x in argon + 0·4 % hydrogen for case 5: $p_0 = 5{\cdot}17$ torr, $T_0 = 297{\cdot}0$ °K, $M_s = 16{\cdot}2$.

Bristow & Glass (1972) first discussed the use of hydrogen addition with a view to eliminating some inexplicable flow disturbances both within and behind the shock-wave structure. The same type of disturbance has been observed at higher Mach numbers for krypton as well (Glass, Liu & Tang 1977). The disturbances are not observed at lower Mach numbers (figure 4). The reason why hydrogen addition can stabilize the flow as indicated by the interferograms is still unknown at this time.

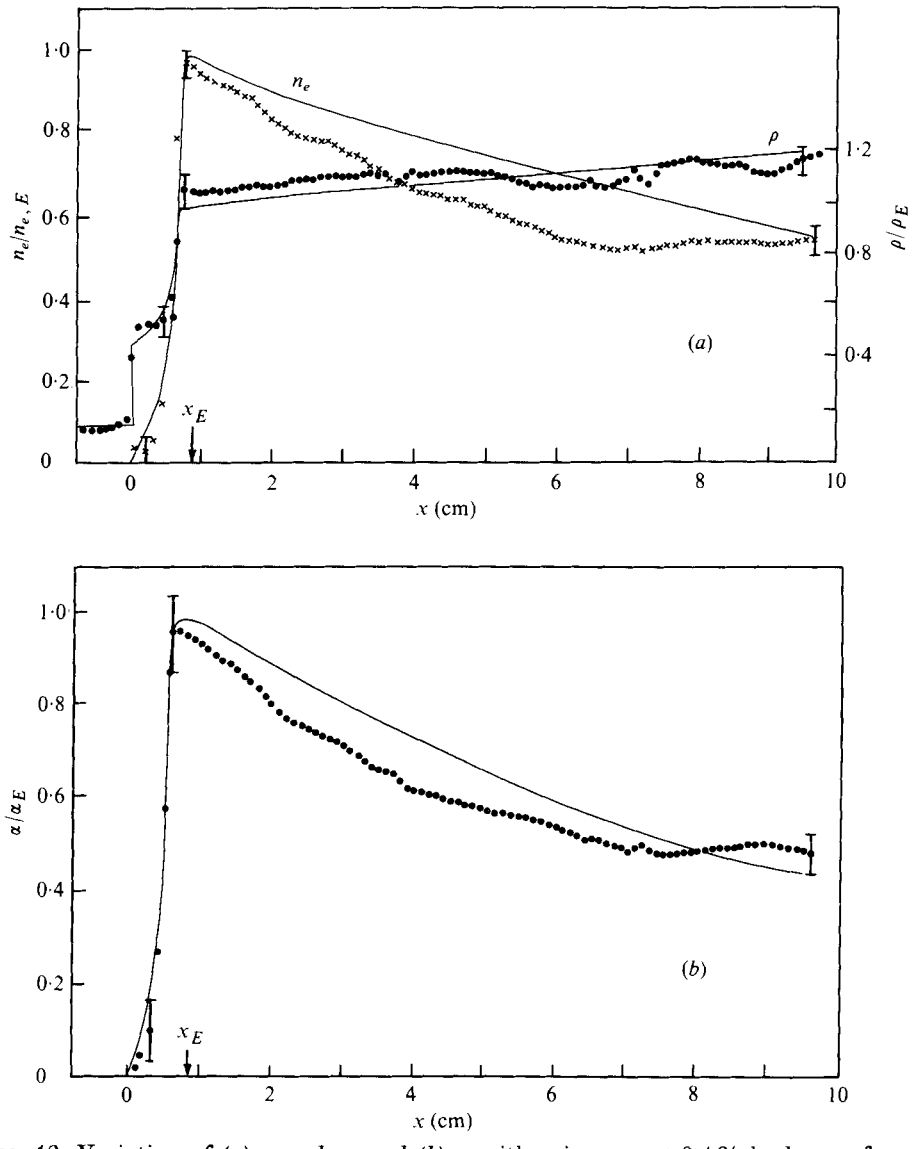

FIGURE 12. Variation of (*a*) ρ and n_e and (*b*) α with x in argon + 0·4 % hydrogen for case 6: $p_0 = 3{\cdot}12$ torr, $T_0 = 298{\cdot}2$ °K, $M_s = 17{\cdot}7$.

Wall effects in relaxation region

An interesting result was found experimentally in the relaxation region near the shock-tube wall as shown very clearly in figure 1 for $\lambda_1 = 6943$ Å, which is sensitive to electron density. It is seen that the front E, where a cascading of electrons occurs, moves in towards the wall slowly at first and then very rapidly. The front is nearly at the translational shock front as the wall boundary layer is reached. Figures 13(*a*) and (*b*) show contours of constant α for shocks ($M = 16{\cdot}5$ and $M_s = 13{\cdot}6$) moving into pure argon obtained by Brimelow (1974). While similar effects are seen in both instances, the phenomenon is much more in evidence for the stronger shock. This might

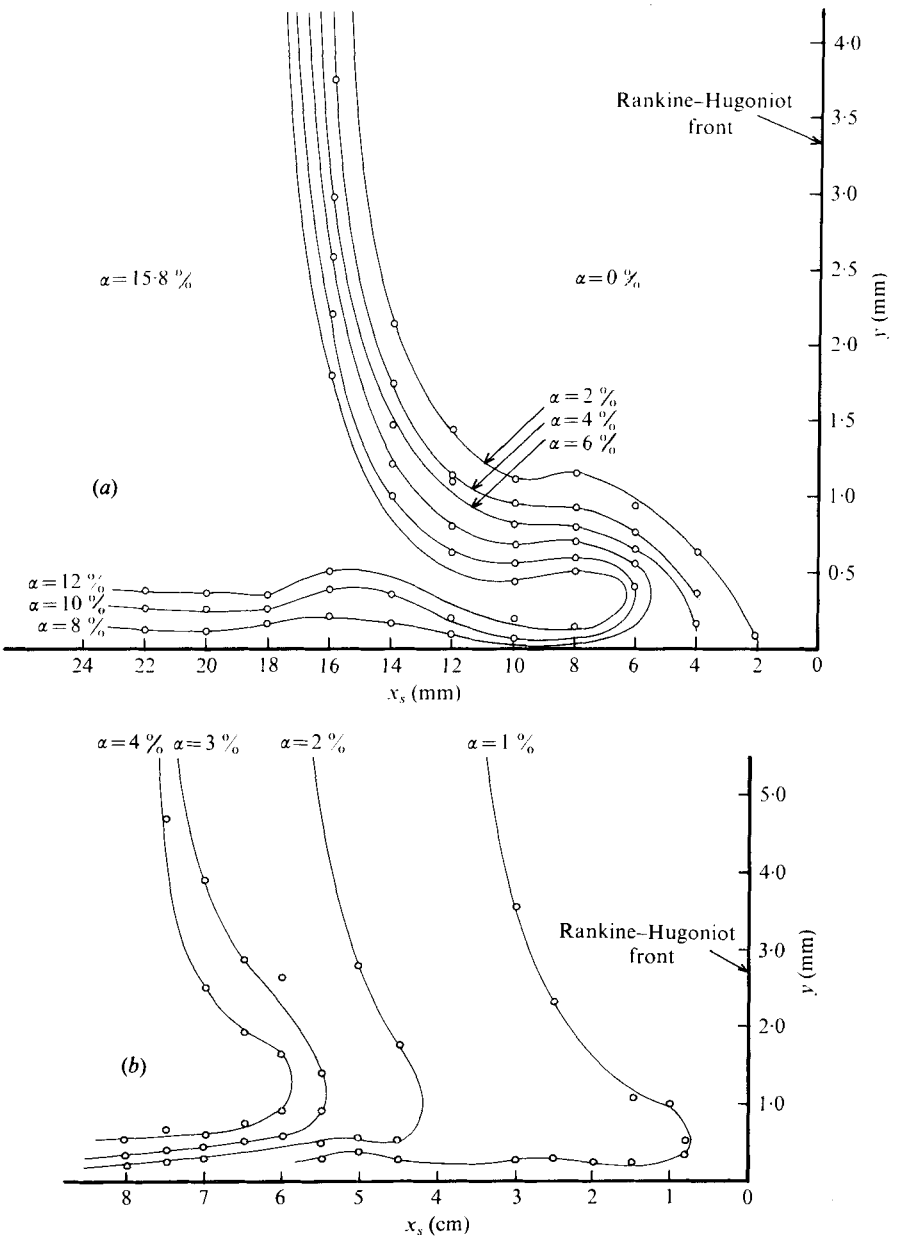

FIGURE 13. Contours of constant degree of ionization in the relaxation region close to the wall for argon. (*a*) $M_s = 16{\cdot}5$, $p_0 = 5{\cdot}12$ torr and $T_0 = 296{\cdot}6$ °K. (*b*) $M_s = 13{\cdot}6$, $p_0 = 5{\cdot}09$ torr and $T_0 = 296{\cdot}7$ °K.

have been expected, as there the electron number density is greater and the relaxation length is much shorter. A similar wall effect occurs with the addition of hydrogen, helium and oxygen impurities (figures 2 and 3) to the argon test gas. In the case of hydrogen, the relaxation region is drastically shortened and only a few fringes supply data in the wall relaxation region. Therefore the change is not so apparent. The

separation between the electron front and the translational shock wave as the boundary layer is approached is about the same in all cases, which is somewhat surprising. A smaller separation might have been expected with the hydrogen impurity.

The reasons for this premature ionization close to the wall are far from clear. One possibility considered was that a gas–surface interaction occurred between the argon plasma and the chromium-plated steel shock-tube wall. Two experiments were carried out to try and eliminate this possibility. In one, a covering (0·008 cm) of ordinary Sellopac (cellophane) tape was stuck to the wall and in the other thin tungsten foil (0·003 cm) was fixed to the wall. It was hoped that the tape, being a good electrical insulator, or the tungsten, having a different work function from chromium or steel, might change the electron distribution, if indeed a gas–surface interaction were taking place. However, no changes were observed (Brimelow 1974).

The possibility of impurities, especially water vapour, being present on any shock-tube surface must also be considered. The wall was cleaned as thoroughly as possible before each experiment. However, the presence of water-vapour molecules, typically at a density of about 10^{14} cm^{-2} at a pressure 10^{-6} torr, might be considered a possible cause, since at the temperature behind the shock front (say 20000 °K) any water-vapour molecules would be completely dissociated and hydrogen, as already proved, has a dramatic effect on the ionization rates. However, it is not clear how their presence would be felt in the free stream close to the wall even after desorption. Yet, as seen from figure 13, the concentration gradient is away from the wall, confirming that it is part of the ionization front, and not due to an impurity concentration gradient, whose effects would be strongest at the wall. In the present experiments an absolute vacuum of 1×10^{-5} torr was obtained with a leak rate of about 10^{-5} torr/min. A mass spectrograph of the adsorbed gases showed that about 50 % was water and the rest air. The water remained constant. It is therefore doubtful if water had a significant effect. Additional experimental tests, such as coating the wall with water and water–salt solution (NaCl) to accentuate water adsorption or provide a readily ionizable substance (Na), were also negative. Admissions of known quantities of water vapour have been tried very recently as noted above. They stabilized the transition as readily as hydrogen and made no apparent change in the approach of the electron–cascade front to the translational front near the wall (Tang 1977). It is therefore concluded that this effect is not due to water vapour.

The effects of the viscous boundary layer on the shock-tube wall is another consideration. It is not clear, however, how the wall boundary layer interacts with and affects the gross features of ionizing shock waves except to shorten the relaxation length as shown by Enomoto (1973).

5. Conclusions

The use of dual-wavelength interferometry has proved to be an excellent method for investigating ionizing shock-wave structure in argon. The measurements of total density and electron number density in the relaxation region show good agreement with a theoretical fit that provides a more precise value of $S^*_{\mathrm{Ar\,Ar}} = 1{\cdot}0 \times 10^{-19}$ cm^2/eV at $M_s \sim 16$ and $p_0 \sim 5$ torr which is close to the value $1{\cdot}2 \times 10^{-19}$ cm^2/eV determined by Kelly (1966) and larger than the value $2{\cdot}5 \times 10^{-20}$ cm^2/eV given by McLaren & Hobson (1968). Nevertheless, it is not absolutely certain whether this value is applicable for all

initial pressures and Mach numbers. For example, for our data a value of 2×10^{-19} cm^2/eV provides a better fit for the case $M_s \sim 13$ and $p_0 \sim 3$ torr.

The radiative-cooling losses are important for high Mach number shock waves at higher pressures. The flow velocity, the electron temperature and the atom temperature decrease monotonically throughout the radiative-cooling region, whereas the density and pressure increase.

Owing to the low mass of the hydrogen atom and the large excitation cross-section constants for hydrogen atom–atom and hydrogen atom–electron colllsions, even a small addition (0·4 %) of hydrogen to the argon test gas as an impurity drastically reduces the relaxation length. The addition of hydrogen is required to remove the sinusoidal-type instabilities from the translational shock front as well as those from the ionization front and the subsequent free stream. How hydrogen or water vapour removes these instabilities has as yet not been explained, despite the accurate analytical predictions of the profiles of the density, electron concentration and degree of ionization. The sinusoidal instabilities investigated here may offer some important clues to the abatement of instabilities leading to detonations and explosions.

It should be noted that the present experiments are not in a Mach number range where real-gas effects cause the second derivative $(\partial^2 p/\partial v^2)_s$ of pressure with respect to volume at constant entropy to become negative, in violation of the second law of thermodynamics, which would give rise apparently to shock-wave instabilities (see Cowperthwaite 1968; Fowles 1976; Rusakov 1975; Griffiths, Sandeman & Hornung 1976). Consequently, it must be concluded at present that the instabilities are associated with a significant degree of ionization.

Another unsolved problem is the progression of the cascading-electron (ionization) front towards the translational shock front as the shock-tube wall is approached.

It is hoped that the present interferometric profiles will stimulate additional theoretical research on shock-wave stability and premature ionization near the shock-tube walls. In addition, the precise and detailed interferometric data can always be used in future to determine a more universal value of $S^*_{\mathrm{Ar\,Ar}}$ when more accurate values of collision cross-sections for momentum and energy transfer become available. Similar results for krypton may be found in Glass *et al.* (1977).

We are pleased to express our thanks to a number of members of our group whose valuable interferograms were used for this paper. Dr M. P. Bristow first observed the instabilities and conducted many useful experiments to determine possible causes. Mr. P. I. Brimelow conducted experiments on shock structure and the wall boundary layer. We thank Mr B. T. Whitten for his computer-evaluation program for interferograms, photographs of shock waves at lower Mach number diffracting over a sharp corner, his cheerful assistance with all experiments, and valuable discussions. Finally, the painstaking work by Mr F. C. Tang in evaluating all of the interferograms and in conducting many runs in argon and krypton is gratefully acknowledged. The financial assistance received from the Air Force Office of Scientific Research under Grant No. AF-AFOSR-77-3303 and from the National Research Council of Canada is acknowledged with thanks.

REFERENCES

APPLETON, J. P. & BRAY, K. N. C. 1964 *J. Fluid Mech.* **20**, 659.

BELOZEROV, A. N. & MEASURES, R. M. 1969 *J. Fluid Mech.* **36**, 695.

BRIMELOW, P. I. 1974 *Univ. Toronto, Inst. Aerospace Studies Tech. Rep.* UTIAS 187.

BRISTOW, M. P. F. & GLASS, I. I. 1972 *Phys. Fluids* **15**, 2066.

CHANG, C. T. 1966 *Proc. 7th Int. Conf. Phenomena in Ionized Gases*, vol. 2, pp. 742–756. Belgrade: Gradevinska Knjiga Publishing House.

COWPERTHWAITE, M. 1968 *J. Franklin Inst.* **285**, 275.

DEVOTO, R. S. 1967 *Phys. Fluids* **10**, 354.

ENOMOTO, Y. 1973 *J. Phys. Soc. Japan* **35**, 1228.

FOWLES, G. R. 1976 *Phys. Fluids* **19**, 227.

FROST, L. S. & PHELPS, A. V. 1964 *Phys. Rev.* **136**, 1538.

GLASS, I. I., LIU, W. S. & TANG, F. C. 1977 *Can. J. Phys.* **56**, 1269.

GRIFFITHS, R. W., SANDEMAN, R. J. & HORNUNG, H. G. 1976 *J. Phys. D. Appl. Phys.* **9**, 1681.

HARWELL, K. E. & JAHN, R. C. 1964 *Phys. Fluids* **7**, 214, 1554.

HOFFERT, M. I. & LIEN, H. 1967 *Phys. Fluids* **10**, 1769.

HOLLENBACH, P. J. & SALPETER, E. E. 1969 *J. Chem. Phys.* **50**, 4157.

HORN, K. P. 1966 *Stanford Univ. Ref.* SUDAAR 268.

HORN, K. P., WONG, H. & BERSHADER, D. 1967 *J. Plasma Phys.* **1**, 157.

JAFFRIN, M. Y. 1965 *Phys. Fluids* **8**, 606.

KAMINOTO, G. & TESHIMA, K. 1972 *Dept. Aero. Engng, Kyoto Univ. Current Paper* no. 33.

KAMIMOTO, G., TESHIMA, K. & NISHIMURA, N. 1972 *Dept. Aero. Engng, Kyoto Univ. Current Paper* no. 36.

KELLY, A. J. 1966 *J. Chem. Phys.* **45**, 1723.

MCCHESNEY, M. & AL-ATTAR, Z. 1965 *J. Quant. Spectrosc. Radiat. Transfer* **5**, 553.

MCLAREN, T. I. & HOBSON, R. M. 1968 *Phys. Fluids* **11**, 2152.

MEINERS, D. & WEISS, C. O. 1976 *J. Quant. Spectrosc. Radiat. Transfer* **16**, 273.

MERILO, M. & MORGAN, E. J. 1970 *J. Chem. Phys.* **52**, 2192.

MORGAN, E. J. & MORRISON, R. D. 1965 *Phys. Fluids* **8**, 1608.

OETTINGER, P. E. & BERSHADER, D. 1967 *A.I.A.A. J.* **5**, 1625.

PETSCHEK, H. & BYRON, S. 1957 *Ann. Phys.* **1**, 270.

POMERANTZ, J. 1961 *J. Quant. Spectrosc. Radiat. Transfer* **1**, 185.

RUSAKOV, M. M. 1975 *Heat Phys. High Temp.* **13**, 20.

SCHULTZ-GRUNOW, F. 1975 *Z. Flugwiss.* **23**, 51.

SCHULTZ-GUIDE, E. 1970 *Z. Phys.* **230**, 449.

SHERMAN, F. S. 1960 *J. Fluid Mech.* **8**, 465.

TANG, F. C. 1977 M.A. Sc. thesis, Institute of Aerospace Studies, University of Toronto.

TUTTLE, L. & SATTERLY, J. 1925 *The Theory of Measurements*. Longmans.

WHITTEN, B. T. 1977 Ph.D. thesis, Institute for Aerospace Studies, University of Toronto.

ZAPESOCHNYI, I. P. & FELSTON, P. V. 1966 *Opt. Spectrosc.* **20**, 291.